COBEM 2021 26th International Congress of Mechanical Engineering
ABCM Associação Brasileira de Engenharia e Ciências Mecânicas
November 22-26, 2021, Virtual Congress, Brazil

COB-2021-1666
NUMERICAL SIMULATION OF AN AERO DESIGN AIRCRAFT AERODYNAMIC CHARACTERISTICS

Caio Vinícius Schurgelies de Sá
Braulio Gutierrez Pimenta
Departamento de Engenharia Mecânica, Universidade de Brasília. Campus Universitário Darcy Ribeiro, Brasília-DF.
caioschurgelies@gmail.com
brauliogp@unb.br

Abstract. *We present a complete workflow to obtain the aerodynamic characteristics of a SAE Brasil Aero Design Competition aircraft via computational fluid dynamics (CFD). A brief discussion about the computational and numerical resources used is given. The model aircraft is a radio-controlled flying wing, where its basic geometry is introduced for a flow regime with a typical Reynolds number in the range of* 4.5×10^5 *to* 8.5×10^5*. We use the ICEM CFD software for pre-processing, the SU2 open-source simulation code for simulation and the Paraview visulization software for post-processing. A mesh convergence study and a validation of the Spalart-Allmaras (SA) and the Shear Stress Menter (SST) turbulence models to our application are presented. We use the Vortex Lattice Method (VLM) and the three-dimensional Panel Method available in XFLR5 software and experimental data available from literature to decide about the cost-benefit and to assess the level of fidelity of each method. After that, simulations results of longitudinal coefficients, sideslip angle, aileron deflection and ground effect are presented. We conclude that the presented CFD-based workflow is consistent and has good cost-benefit in the context of the detailed project for the SAE Brasil Aero Design Competition, and that it can be also used for similar Unmanned Aerial Vehicle (UAV).*

Keywords: *computational fluid dynamics (CFD), RANS simulation, SU2, UAV*

1. INTRODUCTION

The SAE Brasil Aero Design competition (SAE Brasil, 2011) is a Student's Program which is part of SAE Brasil calendar since 1999. Teams of engineering undergraduate and graduate students, representing their universities, are challenged to conceive, design, build and test a fixed-wing radio-controlled aircraft. The competition is held annually, and is subjected to Rules defined to the corresponding year, such as geometrical and power restrictions.

In the scope of Aerodynamics, it is essential to master one or more methodologies to predict with enough accuracy the aerodynamic characteristics of the airplane. The Vortex Lattice Method (VLM) and the 3D Panels Potential Flow Method are alternatives with low computational cost. Free software implementations with friendly user interface, such as the XFLR5, have the advantage of coupling with XFOIL semi-empirical boundary layer model (Drela, 1989). A Reynolds-averaged Navier–Stokes equations (RANS) based simulation cycle is frequently used at more experienced teams, trying to overcome the the limitations of the lower cost methodologies and guiding the airplane optimization at the detailed design phase. Sparlart-Allmaras (SA) and the Shear Stress Menter (SST) models, respectively with one and two transport equations to model turbulent viscosity, are the most popular ones for this purpose. However, RANS simulations should be used carefully only after a rigorous convergence study of the mesh pattern and validation of the simulation code were carried.

2. METHODOLOGY

2.1 Resources

In this work the ICEM CFD v18.1 was used for mesh generation, the SU2 code, described in Palacios *et al.* (2013), v7.0.5, for the simulations and the Paraview v5.8.0 for post-processing. The simulations were run using the Amadea cluster, located at the Computation Aeroacoustic Laboratory (CaaLab) at the University of Brasília. The cluster has eight processors Intel Xeon Phi KNL as compute nodes with 64 cores and 256 simultaneous threads, adding up to 21.28 Teraflops of computatinal power, 128 GigaBytes of MCDRAM memory and 768 GigaBytes of SDRAM DDR4 memory. There is also one visualization node with 256 Gigabytes of RAM memory, a 64 cores Intel Xeon processor and a Nvidia Quadro P5000 GPU. A GNU/Linux-based operational system is used, with available remote internet access through the master node.

2.2 Prototype aircraft

A conceptual discussion of an Unmanned Aerial Vehicle (UAV) flying wing can be found in Alexandrou *et al.* (1993). The data present in this work refers to a prototype of Draco Volans Aerodesign, shown in Fig. 1 and Fig. 2. The reference area is $S_{ref} = 1.45\,\mathrm{m}^2$, the reference chord is $c_{ref} = 0.609\,\mathrm{m}$ and the reference wingspan is $b_{ref} = 2.428\,\mathrm{m}$. The prototype has elevons and drag rudders for control and endplates for stability.

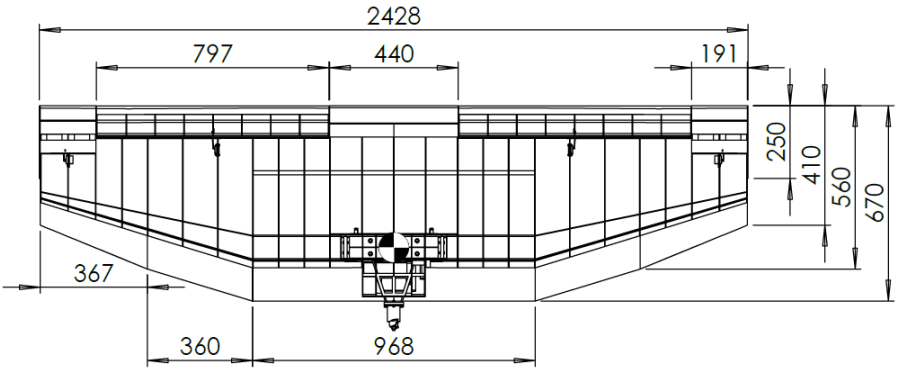

Figure 1. Top view with dimensions in millimeters.

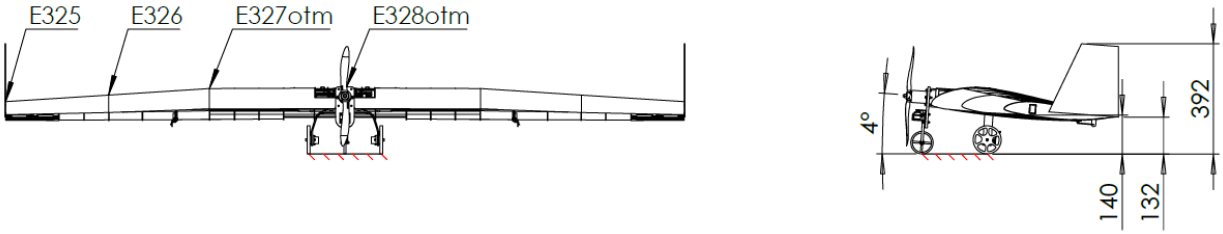

Figure 2. Front and side views with dimensions in millimeters.

2.3 Aerodynamics coefficients definition

We must first introduce some standard coefficients in order to do not cause any misunderstand in the results interpretation. The Reynolds number *Re* is based on c_{ref}. Using the dynamic pressure

$$q_\infty = \frac{1}{2}\rho U_\infty^2, \tag{1}$$

where ρ is the air density and U_∞ is the free-stream velocity, we define the pressure coefficient

$$C_p = \frac{p - p_\infty}{q_\infty}, \tag{2}$$

where p_∞ is the free-stream pressure and p is the pressure at the position of interest, and the skin friction coefficient

$$C_f = \frac{\tau_w}{q_\infty}, \tag{3}$$

where τ_w is the wall shear stress. Throughout this text, we will provide the aerodynamic characteristics in term of dimensionless coefficients based on wind axes (Drela, 2014). Drag, lateral force and lift coefficients are defined, respectively, as

$$C_D = \frac{D}{q_\infty S_{ref}}, \tag{4}$$

$$C_Y = \frac{Y}{q_\infty S_{ref}}, \tag{5}$$

$$C_L = \frac{L}{q_\infty S_{ref}}, \tag{6}$$

where D is drag, Y is lateral force and L is lift. Similarly, we define the rolling, pitching and yawing moment coefficient as, respectively:

$$C_\ell = \frac{\mathcal{L}}{q_\infty S_{ref} b_{ref}}, \tag{7}$$

$$C_M = \frac{\mathcal{M}}{q_\infty S_{ref} c_{ref}}, \tag{8}$$

$$C_N = \frac{\mathcal{N}}{q_\infty S_{ref} b_{ref}}, \tag{9}$$

where $\mathcal{L}$ is the rolling moment, $\mathcal{M}$ is the pitching moment and $\mathcal{N}$ is the yawing moment.

3. RESULTS

As far as the authors are aware, open access literature lacks of detailed wind tunnel data of finite wings with Reynolds numbers at the range of 5×10^5 to 1.0×10^6. High speed aerodynamics data, where compressible effects are important, can be much more easily found than low Reynolds data. The study of Ananda *et al.* (2012) is the closest that can be found to our Reynolds range of interest, where a rectangular wing with aspect ratio $A = 4$ and Wortmann FX 63-137 profile is tested at $Re = 1.0 \times 10^5$.

3.1 Mesh convergence study

The four grids generated were named coarse, medium, fine and extra fine. We used hybrid grids, with prism layer to capture the boundary layer gradients and tetrahedral cells in the rest of the volume. Surface elements are triangular. A good practice is to use some analytical correlation between Reynolds number and boundary layer thickness δ to determine total prism layer thickness, as cited in (Goetten *et al.*, 2019). At this study we used

$$\delta = 0.37 x Re^{-0.2} \tag{10}$$

where x is the position of the developed boundary layer. We used $x = c_{ref}$, ensuring boundary layer is captured at the trailing edge, with some overestimation at the leading edge. The $y+$ non-dimensional wall distance varied with refinement, being equal to 0.7 in the fine mesh.

The boundary conditions are non-slip at the wing surface, farfield at the domain boundaries and symmetry, since only the semispan is necessary. A bullet-shaped domain was used, the natural extension of the classical C-shape domain used in two-dimensional simulations. The domain dimensions were based on the reference chord c_{ref}, with 50 chord units in the wake direction and 20 to the radius of the C-shaped portion.

The fine mesh, as can be seen in Fig. 3, was considered suitable for the desired application. It consists of $\sim 1.2 \times 10^7$ elements, with a 0.5% drag difference to the extra fine mesh, with $\sim 2.0 \times 10^7$ elements, equivalent to 7 drag counts. The convergence analysis was made with $\alpha = 10°$, where α is the angle of attack.

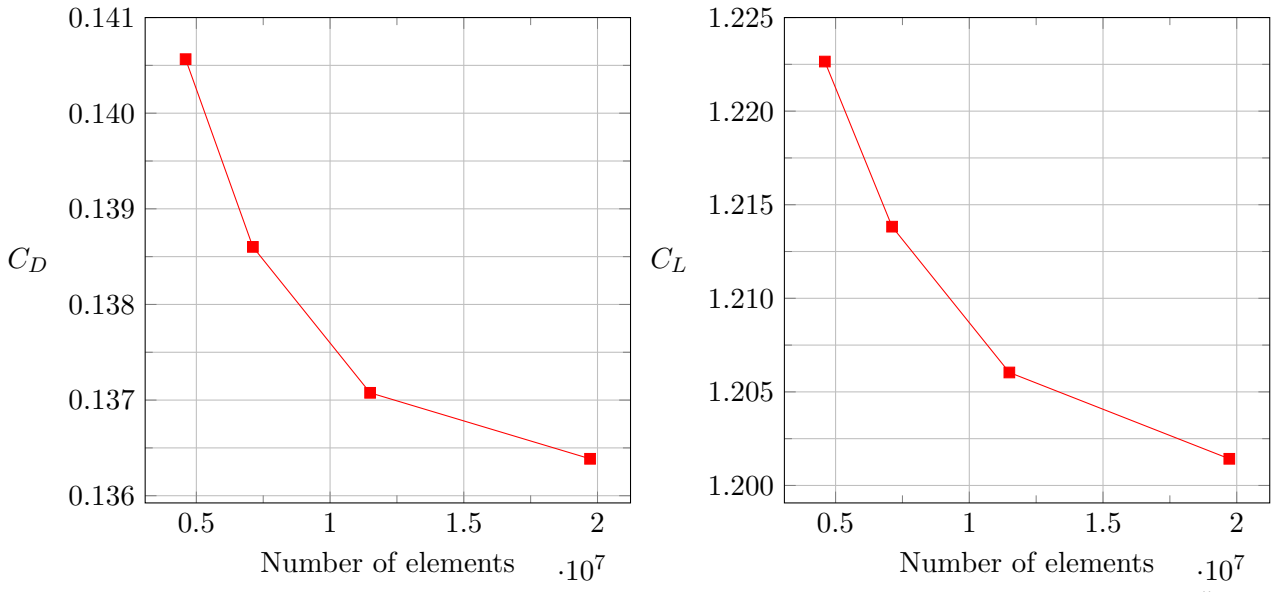

Figure 3. Convergence study to model meshes named coarse, medium, fine and extra fine, $\alpha = 10°$, $Re = 6.5 \times 10^5$, SST.

3.2 Validation study

As discussed earlier, the most suitable wind tunnel data available were found on Ananda *et al.* (2012). However, its excessively low Reynolds number of 1.0×10^5 is not fully appropriate to a comparison with a Spalart-Allmaras (SA) or Shear-Stress Menter (SST) simulation, due to the fully turbulent approach used. For that reason, the RANS simulations were compared not only to the $Re = 1.0 \times 10^5$ experimental data but also to Vortex Lattice Method (VLM) and 3D Panel Method results with a more suitable $Re = 6.5 \times 10^5$. Results for lift, pitching moment and drag coefficients can be seen in Fig. 4, Fig. 5 and Fig. 6.

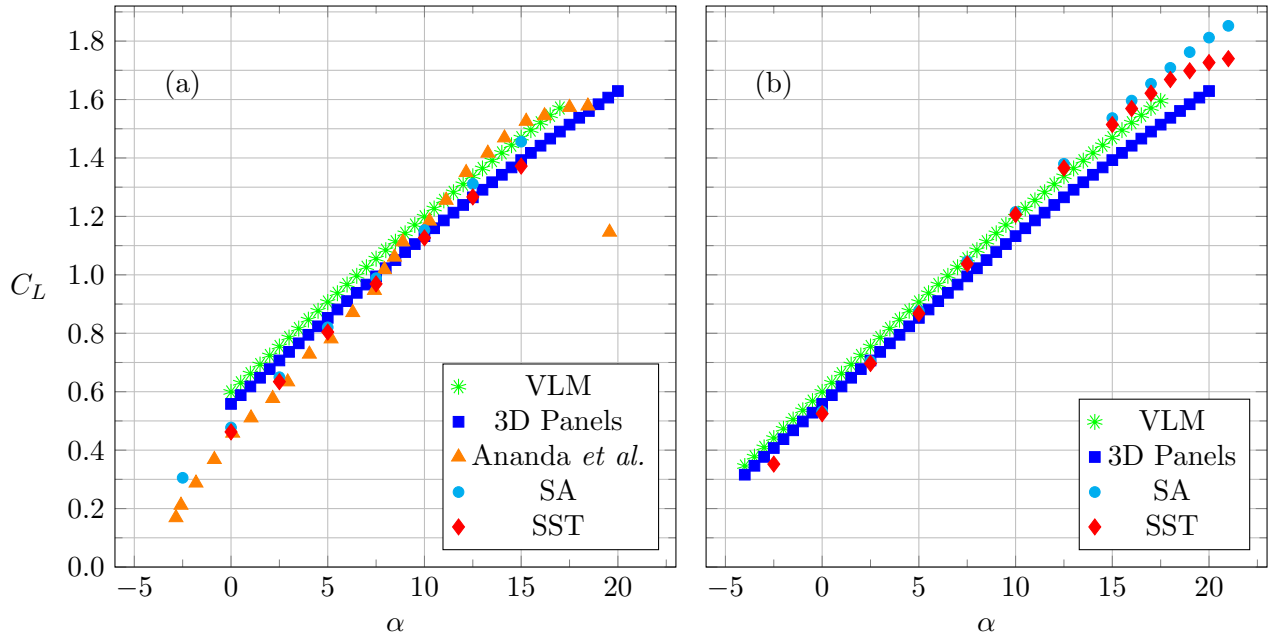

Figure 4. Lift coefficient, aspect ratio $A = 4$, $Re = 1.0 \times 10^5$ (a) and $Re = 6.5 \times 10^5$ (b).

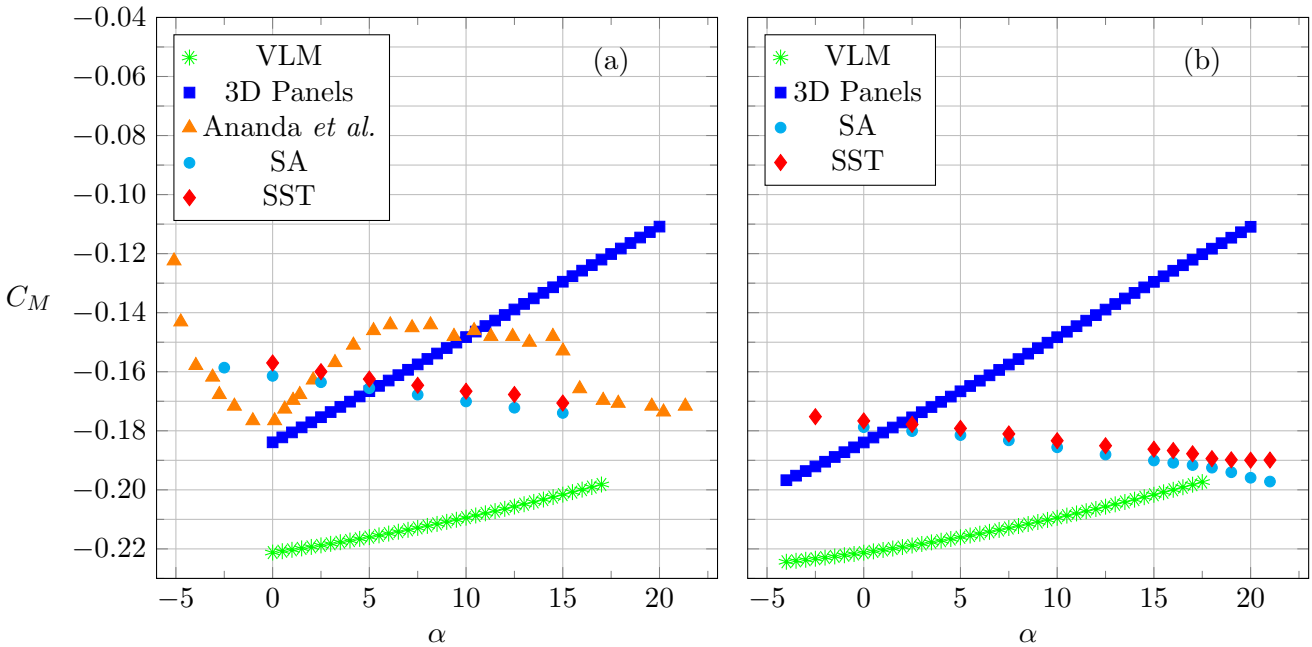

Figure 5. Pitching moment coefficient, referenced to the quarter chord, aspect ratio $A = 4$, $Re = 1.0 \times 10^5$ (a) and $Re = 6.5 \times 10^5$ (b).

Figures 4 and 5 show that even at $Re = 1.0 \times 10^5$ RANS methods fit better the lift derivative $\mathrm{d}C_L/\mathrm{d}\alpha$ and the pitching moment, in comparison to experimental data. For stall and drag (see Fig. 6), the potential methods results are in better agreement with wind tunnel data, what was attributed to the limitations of RANS methods at such low Reynolds. In the

analysis of $Re = 6.5 \times 10^5$, potential and RANS methods lead to closer results, suggesting that at this Reynolds the fully turbulent models are appropriate.

As can be seem in Fig. 5 the moment coefficients does not agree with the experimental results on almost all the methods used in this work. Not even the curve behavior can be observed for the VLM and the 3D Panels methods. This is probably due to excessive simplifications that remove the inherent flow effects. The RANS simulations capture, at a reasonable range of higher angle of attack, the general trend of the moment coefficient at around 5 to 15 degrees. At low angle of attack a similar behavior to the VLM and 3D Panel methods can be observed, although supposedly non-physical. A probable hypothesis that can be made is the laminar-turbulent transition point of the boundary layer throughout the wing being wrongly captured by the RANS models used in this work, even though the lift and drag coefficients were in good agreement with the experimental results.

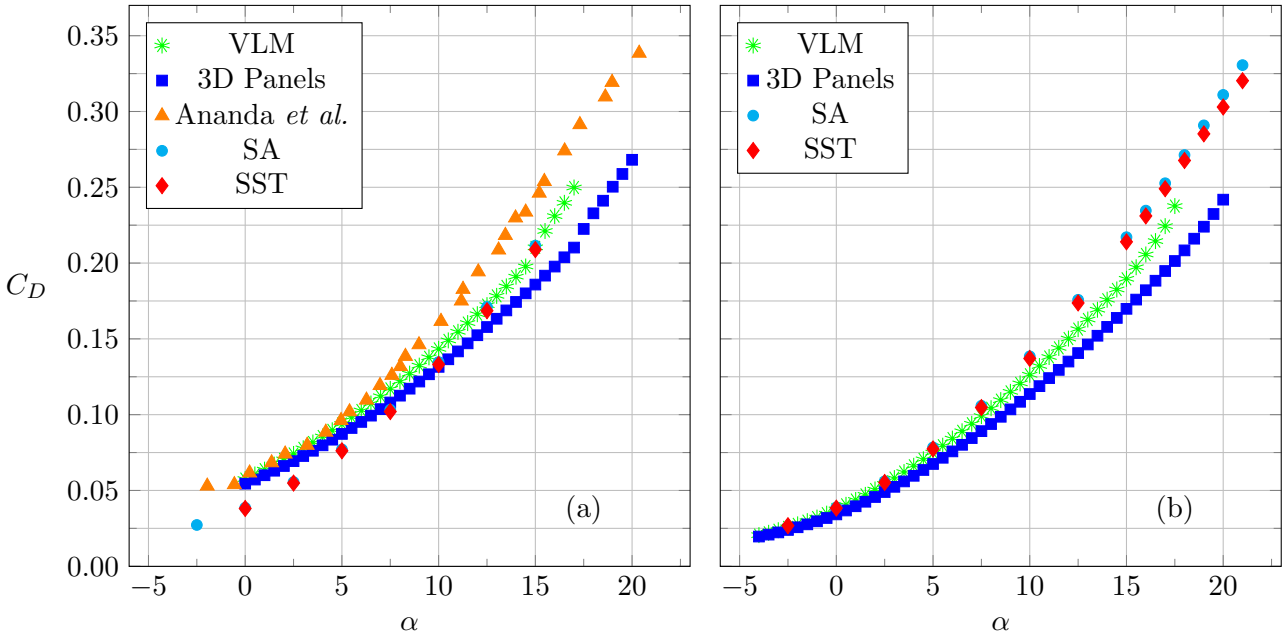

Figure 6. Drag coefficient, aspect ratio $A = 4$, $Re = 1.0 \times 10^5$ (a) and $Re = 6.5 \times 10^5$ (b).

3.3 Longitudinal analysis

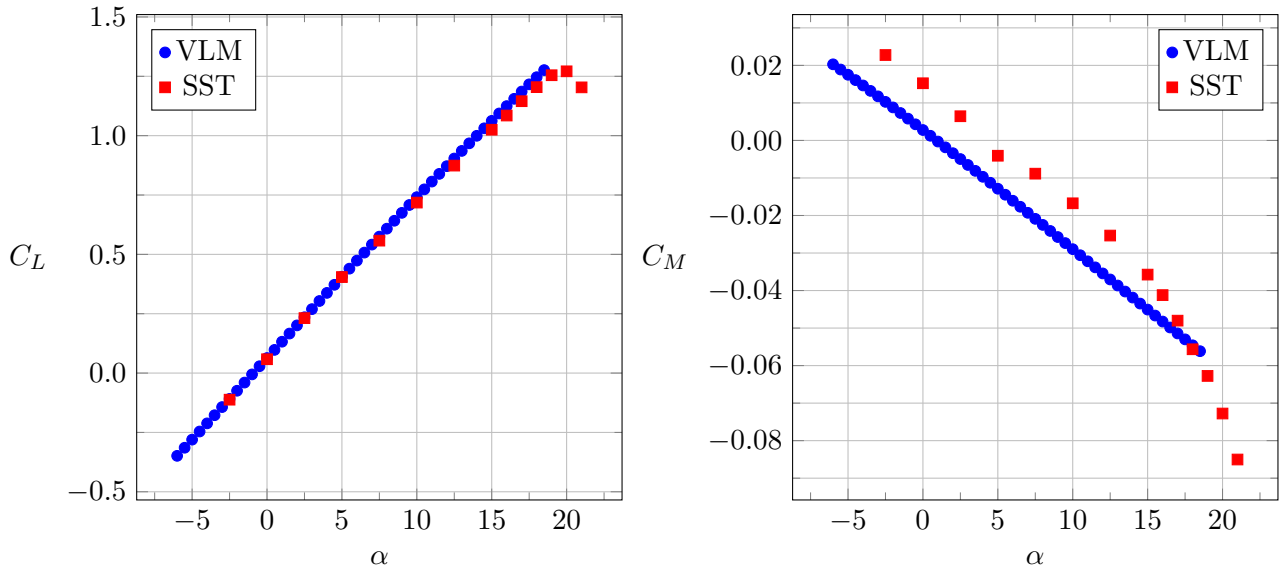

Figure 7. Lift and moment (based on center of gravity) coefficients for the wing with endplates, $Re = 6.3 \times 10^5$.

After the convergence and validation study, the grid generation technique can be applied to obtain the aerodynamic characteristics of the model aircraft, with a higher level of confidence.

For longitudinal analysys, the lift curves were in excellent agreement for VLM and SST, as shown in Fig. 7. Maximum lift coefficients were 1.28 for VLM and 1.27 for SST. The simulations were run, whenever possible, as restarts of previous ones, with smaller angle steps in stall proximity, to avoid divergence. The momentum curves, this time based on the aircraft center of gravity, were also in excellent agreement. The boundary conditions are the same of convergence study.

3.4 Side-slip angle

To understand the influence of side-slip angle β, the full span was simulated, with results shown in Fig. 8 and Fig. 9. It is not expected that potential methods capture the side-slip angle effects with good accuracy, due to boundary layer detachment at the vertical surfaces. The Spalart-Allmaras and Shear Stress Menter simulations can be used to achieve this goal with more fidelity.

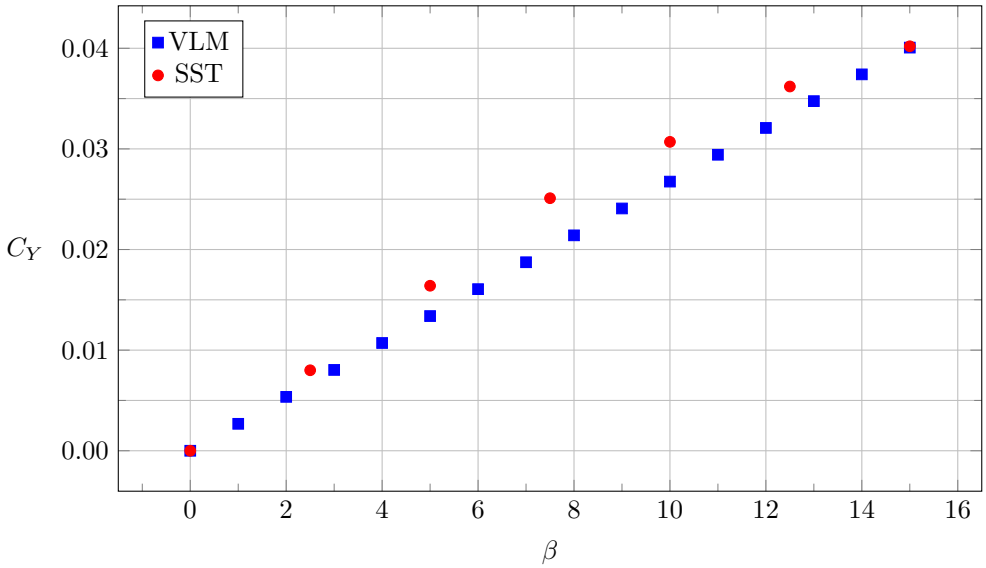

Figure 8. Lateral force coefficient with lateral wind, $\alpha = 0°$, $Re = 8.5 \times 10^5$.

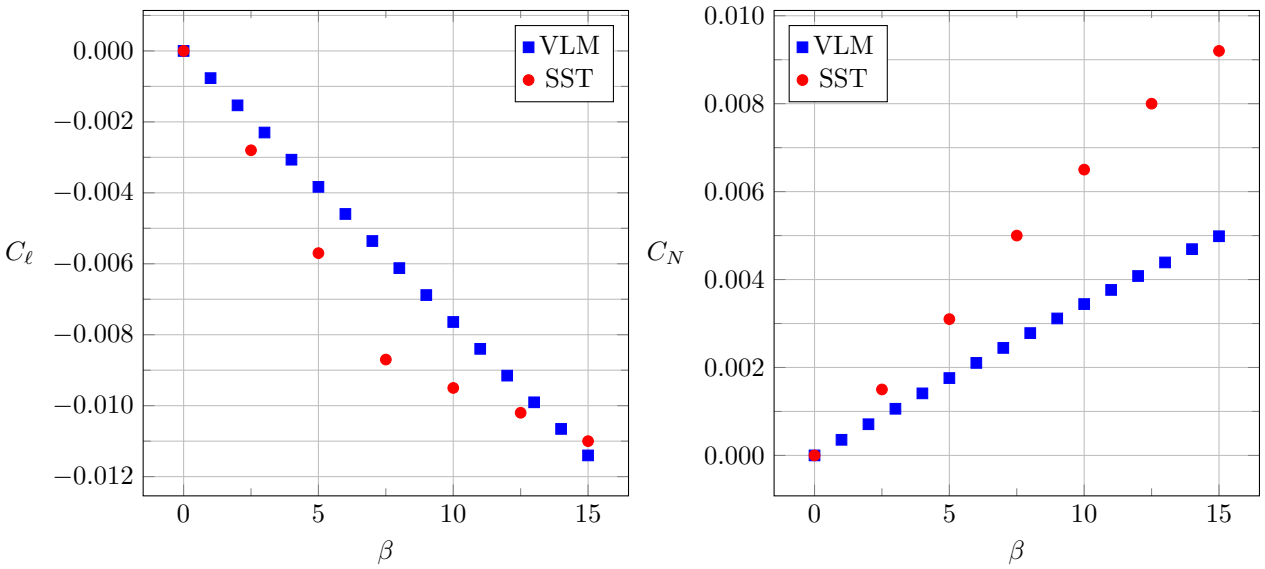

Figure 9. Rolling and yawing moment coefficients based on gravitational center, lateral wind, $\alpha = 0°$, $Re = 8.5 \times 10^5$.

3.5 Control-surface deflection

Elevon deflection, denoted by the angle δ_e, where the upward deflection corresponds to a negative sign, was also simulated. The boundary conditions are the same of the convergence study. The elevon exerts the functions of aileron and elevator combined. The results are shown in Fig. 10. An approximately linear behaviour of lift and moment coefficients, with respect to angle of attack and elevon deflection was found, and hence the $C_L(\alpha)$ of the trimmed aircraft can be

derived as

$$C_L(\alpha) = C_{L0} - \frac{C_{M0}}{C_{M\delta}} C_{L\delta} + \alpha \left(C_{L\alpha} - \frac{C_{M\alpha}}{C_{M\delta}} C_{L\delta} \right), \tag{11}$$

where the $_0$ subscript indicates evaluation at $\alpha = \delta_e = 0$ and α and δ as subscripts indicate derivatives. Therefore, trim reduces the $C_{L\alpha}$, with good agreement between VLM and SST. It was also found that the drag coefficient is basically determined by the lift coefficient. Both results are shown in Fig. 11.

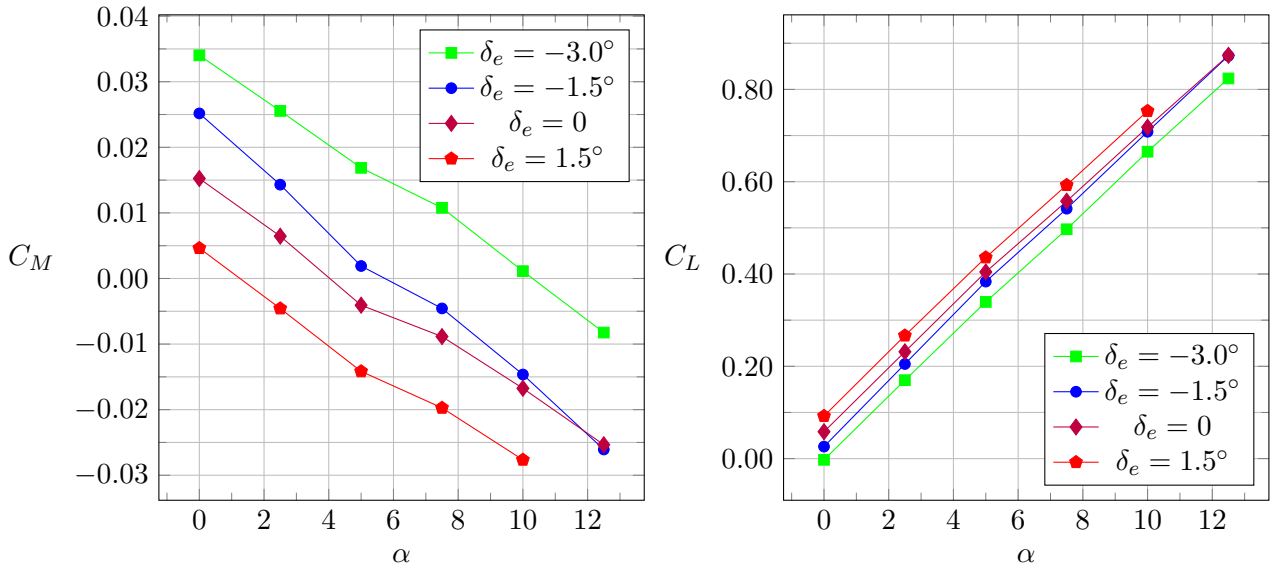

Figure 10. Pitching moment and lift coefficients with elevon deflection, $Re = 6.3 \times 10^5$, SST.

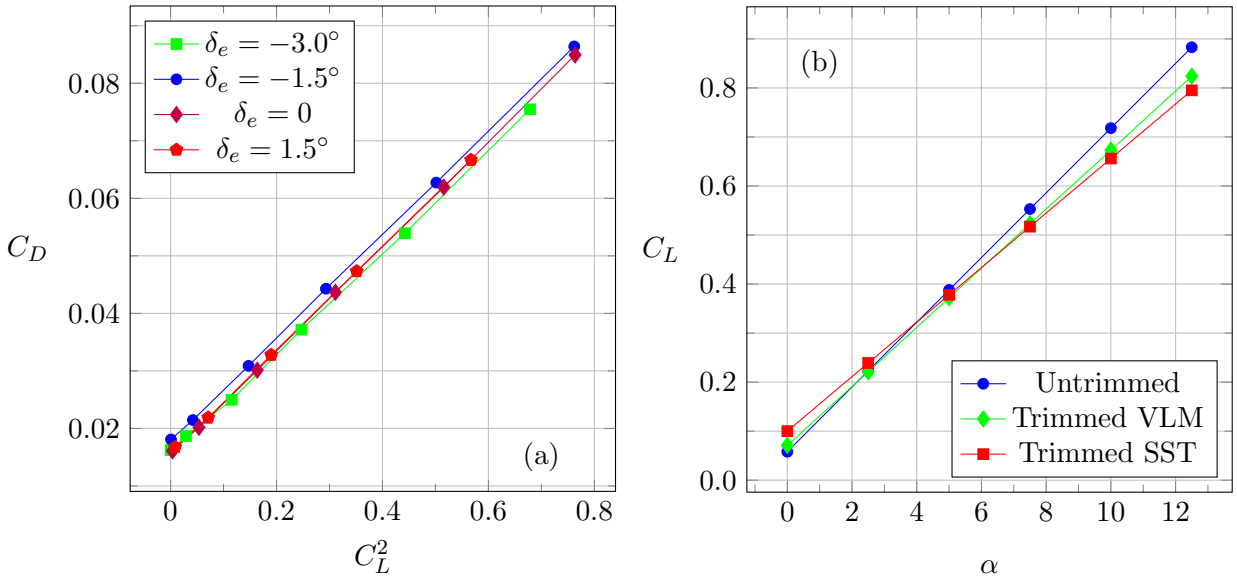

Figure 11. Drag coefficient with elevon deflection (a), SST, and trimmed $C_L(\alpha)$ (b), $Re = 6.3 \times 10^5$.

3.6 Ground effect

Ground effect was simulated with the aircraft height (Fig. 2) for takeoff performance evaluation. For the SST simulation, a moving wall boundary condition was used to represent the ground. At XFLR Vortex Lattice Method, a mirror image of the aircraft under the ground plane is created to impose impenetrability condition, as suggested in Katz and Plotkin (2001). The results, shown in Fig. 12 and Fig. 13, imply a more optimistic lift gain for XFLR5 VLM.

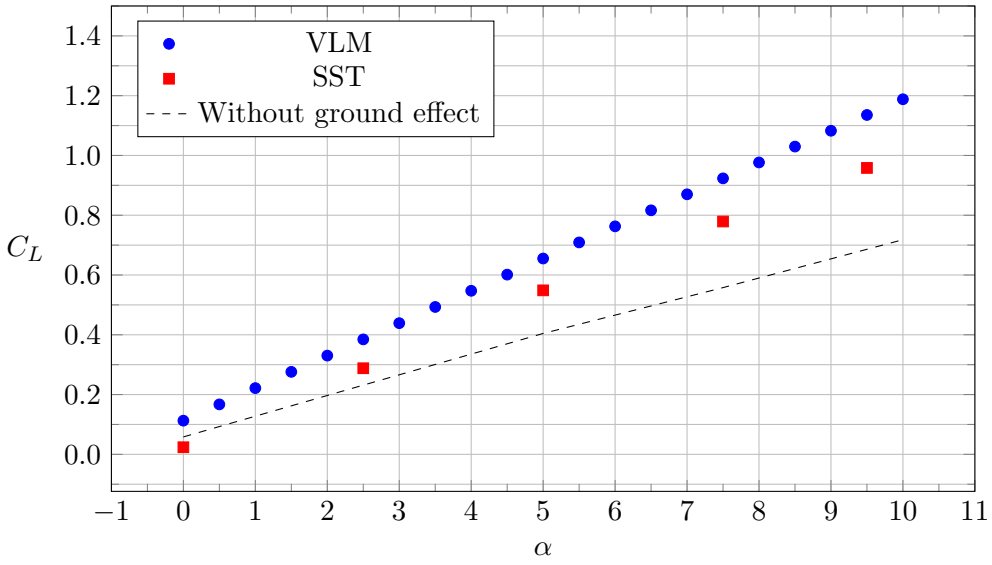

Figure 12. Lift coefficient for ground effect, $Re = 4.8 \times 10^5$.

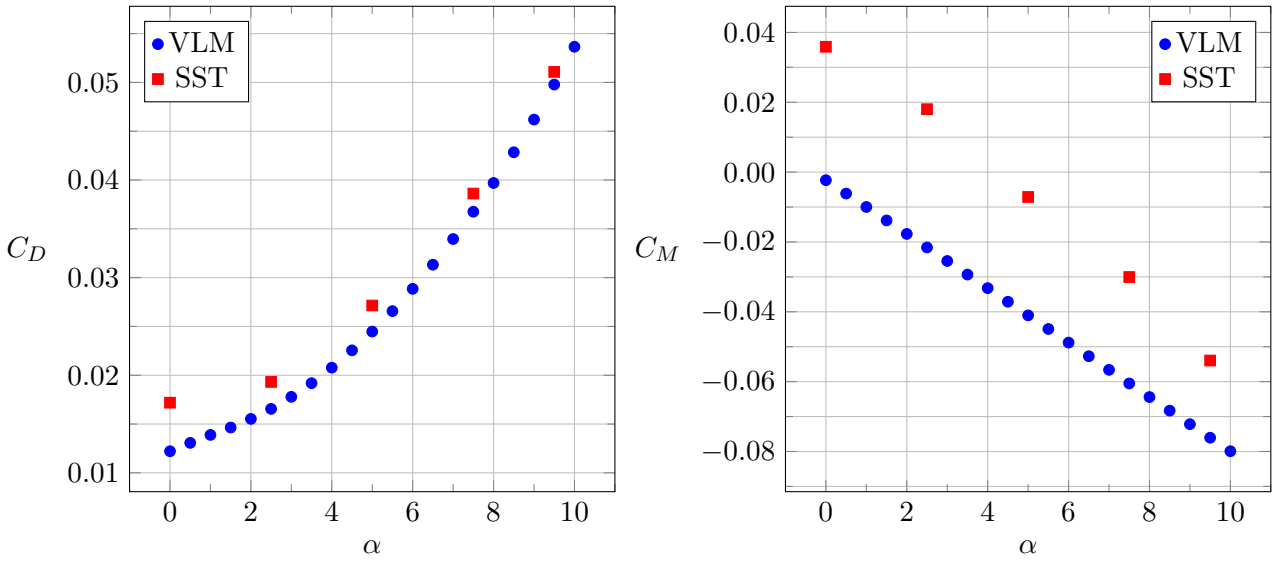

Figure 13. Drag and pitching moment coefficients for ground effect, $Re = 4.8 \times 10^5$.

4. CONCLUSION

The study showed that in order to achieve high convergence levels on RANS simulations, for instance errors less than 10 drag counts, meshes in the order of 10^7 elements may be required for a typical SAE Aero Design aircraft. To the majority of nowadays personal computers, meshes of this extent inhibit a wide simulations campaign, with control surface deflection, for instance. Therefore, a computational cluster remains the most viable solution to RANS simulations even for incompressible and with reduced Reynolds number flows.

Except for mesh generation, with the ICEM CFD software, all the resources used on this work were open source. There are certainly some alternatives for freely available mesh generators, but in the authors evaluation, those lack in robustness compared to the commercial ones, considering the fairly complex meshes required for some SAE Aero Design geometries. Therefore, mesh generation stills is a bottleneck to a fully open source simulation workflow.

A good agreement between VLM and SST simulations for longitudinal coefficients and low control surface deflection showed that, even for its model simplicity, the XFLR5 can be used with an acceptable level of confidence for basic performance analysis and initial design. The RANS simulations are particularly useful for the advanced design phase, to validate geometric optimizations and for better performance assessment for instance.

5. ACKNOWLEDGEMENTS

We thank Draco Volans Aero Design for the support throughout all this research, specially Luís Serra for the CAD models.

6. REFERENCES

Alexandrou, A., Durgin, W., Olinger, D., Crivelli, P., Boucher, M., Carvajal, H., Frank, B., Hill, B., Hilliard, B. and Jeffers, M., 1993. "Design and analysis of a radio-controlled flying wing aircraft".

Ananda, G., Sukumar, P. and Selig, M., 2012. "Low-to-moderate aspect ratio wings tested at low Reynolds numbers". In *30th AIAA applied aerodynamics conference*. p. 3026.

Drela, M., 1989. "Xfoil: An analysis and design system for low Reynolds number airfoils". In *Low Reynolds number aerodynamics*, Springer, pp. 1–12.

Drela, M., 2014. *Flight Vehicle Aerodynamics*. MIT Press.

Goetten, F., Finger, D., Marino, M., Bil, C., Havermann, M., Braun, C. *et al.*, 2019. "A review of guidelines and best practices for subsonic aerodynamic simulations using RANS CFD". In *APISAT 2019: Asia Pacific International Symposium on Aerospace Technology*. Engineers Australia, p. 227.

Katz, J. and Plotkin, A., 2001. *Low-speed aerodynamics*, Vol. 13. Cambridge University Press.

Palacios, F., Alonso, J., Duraisamy, K., Colonno, M., Hicken, J., Aranake, A., Campos, A., Copeland, S., Economon, T., Lonkar, A. *et al.*, 2013. "Stanford university unstructured (SU2): an open-source integrated computational environment for multi-physics simulation and design". In *51st AIAA Aerospace Sciences Meeting Including the New Horizons Forum and Aerospace Exposition*. p. 287.

SAE Brasil, 2011. "SAE Brasil AeroDesign (in Portuguese)". https://saebrasil.org.br/programas-estudantis/aero-design-sae-brasil/. Accessed 12 June 2021.

7. RESPONSIBILITY NOTICE

The authors are solely responsible for the printed material included in this paper.